RESEARCH ARTICLE

Check for updates

Trioxotriangulene with carbazole: a donor–acceptor molecule showing strong near-infrared absorption exceeding 1000 nm†

Tsuyoshi Murata, [ID] [a] Kazuki Kariyazono,[b] Shusaku Ukai,[a] Akira Ueda, [ID] [c] Yuki Kanzaki,[d] Daisuke Shiomi,[d] Kazunobu Sato, [ID] [d] Takeji Takui [ID] [d] and Yasushi Morita [ID] *[a]

A donor–acceptor type trioxotriangulene (**TOT**) neutral radical derivative having three carbazolyl groups as electron-donors was newly synthesized. The ESR spectrum showed that the electronic spin delocalized over both the **TOT** skeleton and three carbazolyl groups, causing high stability of the neutral radical species. In the cyclic voltammetry measurement, the adduct exhibited multiple redox waves from the redox processes of **TOT** from the monocation to radical tetraanion species and also from the oxidation of the carbazolyl groups. The UV-vis spectra showed a strong near-infrared photoabsorption band with an absorption maximum of 1028 nm, which was characterized as an intramolecular charge-transfer from the carbazolyl group to the **TOT** neutral radical core. In both solution and solid states, the neutral radical formed a π-dimer stabilized by the strong two-electron-multicenter bonding on the **TOT** skeleton.

Introduction

Organic molecules that contain electron–donor (D) and electron–acceptor (A) units (D–A) are of interest in the development of organic electronics due to the intramolecular electron transfer (IET) processes which have various applications such as non-linear optics,[1] photovoltaics,[2] photoconductivity,[3] ambipolar charge-transport[4] *etc*. In particular, a strong IET absorption band with a large bathochromic shift extending into the near-infrared (NIR) region is the most characteristic feature of D–A molecules.[5] The wavelength of the IET absorption band can be controlled by the strength of D and A units (HOMO and LUMO energies, respectively), and many D–A molecules having an absorption maximum λ_{max} of 500–900 nm have been reported.[5] On the other hand, D–A type small molecules exhibiting a IET band with $\lambda_{max} >$ 1000 nm are rare.[6,7] When the D or A unit possesses an

unpaired electron, additional intriguing functions can be found, originating from the electronic-spin and open-shell electronic structure. D–A molecules with the perchlorotriphenylmethyl (PTM) neutral radical as an A unit and tetrathiafulvalene (TTF) as a D unit exhibit a high electrical conductivity induced by high pressure (Fig. 1).[8] A TTF derivative having a
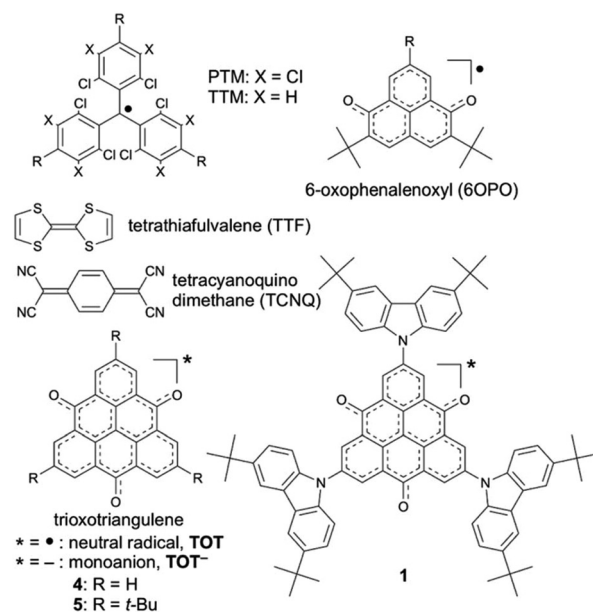
[a]*Department of Applied Chemistry, Faculty of Engineering, Aichi Institute of Technology, Toyota, Aichi 470-0392, Japan. E-mail: moritay@aitech.ac.jp*
[b]*Department of Chemistry, Graduate School of Science, Osaka University, Toyonaka, Osaka 560-0043, Japan*
[c]*Department of Chemistry, Kumamoto University, 2-39-1 Kurokami, Chuo-ku, Kumamoto 860-8555, Japan*
[d]*Department of Chemistry and Molecular Materials Science, Graduate School of Science, Osaka City University, Sumiyoshi-ku, Osaka, 558-8585, Japan*
†Electronic supplementary information (ESI) available: Detailed synthetic procedures of the intermediates, and additional experimental data and molecular orbital energy calculations. CCDC 1894816. For ESI and crystallographic data in CIF or other electronic format see DOI: 10.1039/c9qo00663j

Fig. 1 Molecules in text. R represents the substituent groups, and the asterisk (*) represents the electronic states of the **TOT** skeleton.

This journal is © the Partner Organisations 2019

Org. Chem. Front., 2019, **6**, 3107–3115 | 3107

nitronyl nitroxide unit shows a high electrical conductivity of $\sigma_{RT} = 9 \times 10^{-4}$ S cm^{-1} as a single component under ambient conditions, and also exhibits a magnetoresistance response upon the application of a magnetic field.[9] The D–A molecules of the 6-oxophenalenoxyl (6OPO, A unit) neutral radical with TTF exhibit a spin-center transfer phenomenon controlled by the external stimuli, where the spin-center (unpaired electron) moves from 6OPO to TTF units by the IET process.[10] A similar transformation of the electronic-spin structure based on the bistability of open-shell D–A molecules has also been observed in PTM neutral radicals with TTF and ferrocene (Fc) units.[11,12] In addition to the number of substituted D units, the interaction of the π-electronic system between D and A units would also be important for the intensity of the IET bands. These open-shell D–A molecules also exhibit IET absorption bands in the NIR region with $\lambda_{max} > 1000$ nm; however, their intensities are usually very weak ($\varepsilon_{max} < 10^3$ M^{-1} cm^{-1}).[10–12] The triphenylamine substituted PTM derivatives linked through an ethynyl spacer exhibited a strong IET band at $\lambda_{max} = 800$–900 nm, where the intensity of the band increases with the number of substituted D units, from $\varepsilon_{max} = 5$–6 × 10^3 M^{-1} cm^{-1} for the mono-substituted derivative to $\varepsilon_{max} = 12$–17 × 10^3 M^{-1} cm^{-1} for the tri-substituted one.[13]

Trioxotriangulene (**TOT**, Fig. 1) is a stable organic neutral radical with an electronic-spin structure delocalizing on the whole three-fold symmetric 25π-electronic system.[14] The **TOT** neutral radical possesses a strong electron-accepting ability with the redox potential of −0.05 V *vs.* Fc/Fc$^+$, which is close to that of tetracyanoquinodimethane (Fig. 1, TCNQ, $E = -0.11$ V). The strong self-assembling ability of **TOT** forming one-dimensional π-stacking columns induced high electrical conductivities as single component neutral radicals and mixed-valence salts composed of neutral radicals and monoanion species.[15] We have also disclosed that the π-stacking columns of the **TOT** neutral radical in the crystalline state exhibit a strong NIR absorption with $\lambda_{max} > 1000$ nm through intermolecular interactions of the SOMO.[16]

Here we have newly synthesized a D–A type **TOT** neutral radical having three carbazolyl groups as D units, **1** (Fig. 1). Carbazole is a heterocyclic chromophore, and has been widely studied as a building block of organic electronic materials due to its intrinsic photophysical and redox properties.[17] In particular, the electron-donating and charge-transporting abilities of carbazole derivatives have been utilized in the development of organic light-emitting diodes (OLEDs)[18] and photoconductive materials.[19] Open-shell D–A compounds of the tris(2,4,6-trichlorophenyl)methyl (TTM, Fig. 1) neutral radical with carbazolyl groups as D units have demonstrated various intriguing functions such as low-energy photoabsorption/emission,[19] paramagnetic liquid crystallinity[20] and ambipolar charge-transport.[21] In this paper, we disclose the electronic effects of the carbazolyl groups on the electronic spin structure, redox properties and π-stacking structure of **1**. In particular, we emphasize that the introduction of electron-donating groups to the **TOT** neutral radical as substituents gave rise to a

strong NIR photoabsorption with $\lambda_{max} > 1000$ nm with $\varepsilon_{max} > 10^4$ M^{-1} cm^{-1} due to the IET process.
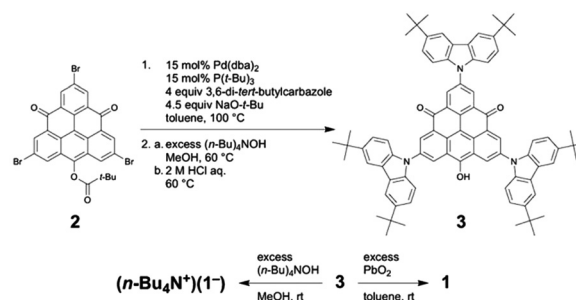
Results and discussion

Synthesis and stability of 1

The synthetic method of **1** is shown in Scheme 1. The carbazolyl groups were introduced into the **TOT** skeleton by the cross-coupling reaction of tribromo **TOT** derivative **2** with corresponding 3,6-di-*tert*-butylcarbazole under the presence of the Pd catalyst.[22] After removing the pivaloyl protecting group with a base, the product was acidified with aqueous HCl to afford the radical precursor **3**. The treatment of **3** with tetra-*n*-butylammonium hydroxide ($(n\text{-Bu})_4\text{N}^+\text{OH}^-$) gave the monoanion salt ($(n\text{-Bu}_4\text{N}^+)(1^-)$), and the oxidation of **3** with PbO$_2$ yielded the neutral radical **1**. Similarly to the pristine **TOT 4**, both ($n\text{-Bu}_4\text{N}^+)(1^-)$ and **1** were stable under air both in solution and in the solid state. Neutral radical **1** did not show any decomposition even at 300 °C under air, and the decomposition point under a N$_2$ atmosphere was ∼400 °C (Fig. S1†).[14d] Due to the bulky *tert*-butyl groups around the carbazolyl groups, **1** was highly soluble in toluene, CH$_2$Cl$_2$ and THF to give a green solution; however, it was insoluble in non-polar hexane and strongly polar DMSO and alcohols.
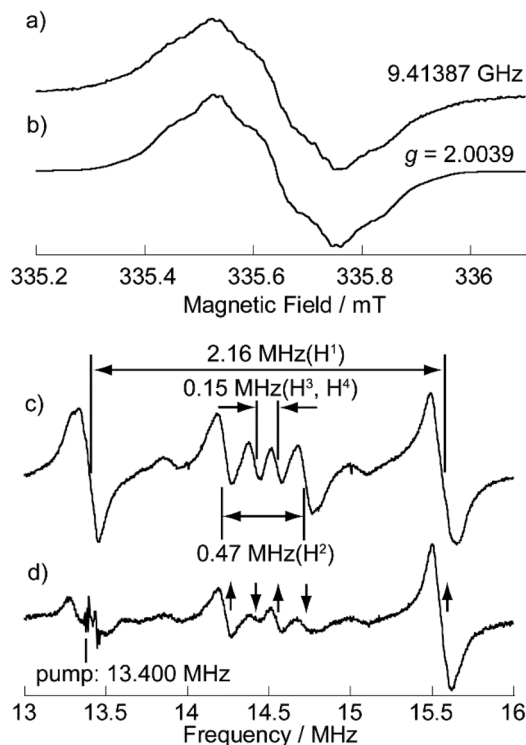
Electronic spin structure

The electronic-spin structure of neutral radical **1** was investigated by ESR and ^{1}H-ENDOR/TRIPLE spectroscopy in toluene solution. The ESR spectrum of **1** showed a broad signal with hyperfine structures owing to the contributions from small hyperfine splitting (Fig. 2a and b). The observed g-value was 2.0040, which is very similar to that of the pristine **TOT 4** ($g = 2.0041$).[14d] The ^{1}H-ENDOR spectrum (Fig. 2c) showed three kinds of proton hyperfine couplings, and their relative signs were unequivocally determined from the ^{1}H-TRIPLE spectrum (Fig. 2d). Considering the molecular symmetry, the observed hyperfine couplings of protons were assigned with the help of DFT calculations (Fig. 3): the largest splitting is assignable to the six α-protons in the **TOT** skeleton ($a(\text{H}^1) = +2.16$ MHz), whereas the smaller ones are ascribable to the protons of the carbazolyl groups ($a(\text{H}^2) = -0.47$ MHz and $a(\text{H}^2) = a(\text{H}^3) = +0.15$ MHz). The experimental and calculated hyperfine coup-

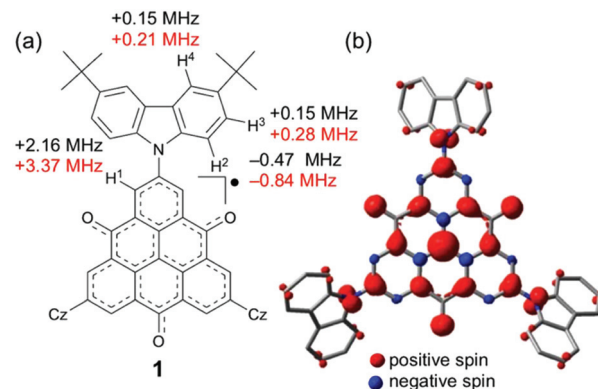**Scheme 1** Synthesis of neutral radical **1** and monoanion salt **1**⁻.

3108 | *Org. Chem. Front.*, 2019, **6**, 3107–3115

This journal is © the Partner Organisations 2019

Fig. 2 (a) Observed at 273 K and (b) simulated ESR spectra, and (c) ^{1}H-ENDOR and (d) ^{1}H-TRIPLE spectra of **1** in degassed toluene (9×10^{-5} M) at 260 K. The ESR simulation was achieved by optimizing the hyperfine coupling constant (hfcc) of the nitrogen nucleus and line width (Lorentzian line shape) with the proton hfcc's (a's) fixed which are experimentally determined by ^{1}H ENDOR spectroscopy: $a(H^1)$ = 2.16 MHz, $a(H^2)$ = 0.47 MHz, $a(H^3)$ = $a(H^4)$ = 0.15 MHz, $a(N)$ = 0.58 MHz and the line width = 0.011 mT (see Fig. S3† for detailed analysis). The upward and downward arrows in (d) denote an increase and decrease in the intensity of an ENDOR signal, respectively, when the pump frequency at 13.400 MHz is applied. Note that the two weak signals appearing at around 13.9 and 15.0 MHz in (c) and (d) are attributable to the unidentified species in extremely small amounts. These signals are free from the TRIPLE effect which is intramolecular, as shown in (d).
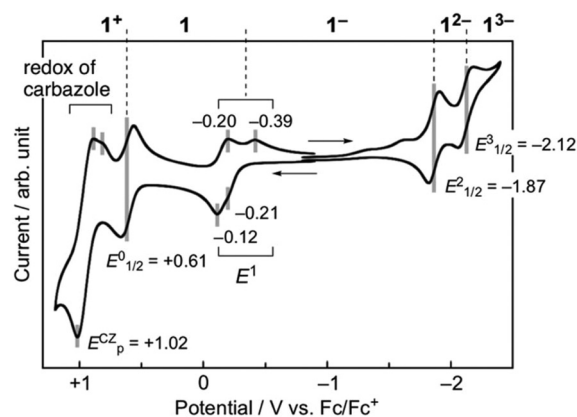

Fig. 3 (a) Observed hyperfine coupling constants (in black) and calculated values (in red) of **1**. Considering the molecular symmetry, the calculated hyperfine coupling constants for the equivalent nuclei were averaged. Cz indicates the 3,6-di-*tert*-butylcarbazolyl groups. (b) Calculated spin-density distribution of **1**. The calculations were performed by using the DFT method at the UB3LYP/6-31G(d,p) level of theory. The *tert*-butyl groups were omitted during the calculation.

Cyclic voltammograms

The electronic effect of the carbazolyl groups on the multistage redox ability was evaluated by means of electrochemical measurements of the salts (n-Bu$_4$N$^+$)(**1**$^-$) in CH$_2$Cl$_2$ (Fig. 4 and Table 1). Due to the poor solubility of the neutral radicals of **4** and **5**, the (n-Bu)$_4$N$^+$ salts of the monoanion species were used for the measurement. In the cyclic voltammetry (CV) measurements in CH$_2$Cl$_2$ (Fig. 4 and Fig. S4†), redox processes of the monoanion **1**$^-$ to radical dianion (**1**$^{2-}$) and further diradical trianion (**1**$^{3-}$) were observed at $E^2_{1/2}$ = -1.87 V and $E^3_{1/2}$ = -2.12 V *vs.* Fc/Fc$^+$, respectively, as reversible ones. On the other hand, the redox wave between monoanion **1**$^-$ and neutral radical **1** at $E^1 \sim -0.2$ V was not simple, where both oxidation and reduction proceeded in two steps probably due to the association of **1**$^-$ and **1** in the solution state. The redox potential of E^1 was much higher than those of TTM

ling constants are in good agreement. These results show that the electronic spin delocalizes over the carbazolyl groups. The delocalization of the electronic spin to the carbazolyl groups is also suggested experimentally from the smaller hyper fine coupling constant of the α-proton on the **TOT** skeleton compared to that of **4** ($a(H^1)$ = 2.57 MHz),[14d] implying the reduction of the electronic-spin density at the α-carbon atoms. In the DFT calculations, 22% of the total spin densities of **1** is located at the three carbazolyl groups. The intensity of the ESR signal of **1** gradually decreased upon cooling due to the formation of a non-magnetic π-dimer as observed in other **TOT** derivatives (Fig. S2†), indicating the strong multicenter bonding nature in the π-dimer of the **TOT** neutral radical.[14d] The enthalpy and entropy changes for the π-dimerization were determined to be -12.9 kcal mol^{-1} and -17.5 eu, respectively, from which the dimerization constant K_{dimer} was determined as 3.7×10^5 M^{-1}.[23] These parameters were similar to those for the tri-*tert*-butyl substituted **TOT 5**, where K_{dimer} is 1.2×10^5 M^{-1}.[16]

Fig. 4 Cyclic voltammograms of **1** measured using the n-Bu$_4$N$^+$ salt of monoanion species (1 mM) in CH$_2$Cl$_2$. The result was calibrated with an Fc/Fc$^+$ couple.

This journal is © the Partner Organisations 2019

Org. Chem. Front., 2019, **6**, 3107–3115 | **3109**

Table 1 Redox potentials (V)[a] of **1**, **4** and **5** in the CV measurements in CH$_2$Cl$_2$ or DMF solution, and their LUMO and SOMO energies (eV)[b]

	1		**4**		**5**	
	CH$_2$Cl$_2$	DMF	CH$_2$Cl$_2$	DMF	CH$_2$Cl$_2$	DMF
E^4	—	-2.75^c	—	-3.09^c	—	-3.18^c
E^3	-2.12	-2.14	—	-2.39	-2.53^c	-2.48
E^2	-1.87	-1.79	-2.18^c	-2.03	-2.18^c	-2.10
E^1	-0.21^c	-0.13^c	$+0.07^c$	-0.05^c	-0.35	-0.26^c
E^0	$+0.61$	$+0.70^c$	—	—	$+0.79^c$	—
E^{cz}	$+1.02^c$	$+0.97^c$	—	—	—	—
LUMO	-2.63^d		-2.53		-2.29	
SOMO	-3.19^d		-3.33		-3.11	

[a] Potentials were calibrated with an Fc/Fc$^+$ couple = 0 V. [b] Calculated by the DFT method at the ROB3LYP/6-31G(d,p) level of theory. [c] Peak potentials were listed due to the irreversibility. [d] Calculated with an optimized structure where the dihedral angle between **TOT** and carbazolyl groups is 47°.

(-0.89 V)[19a] and PTM (ca. -0.7 V),[13] indicating the stronger electron-accepting ability of **1**. At a further higher potential, a reversible wave assignable to the redox between neutral radical **1** and monocation species **1**$^+$ was observed at $E^0_{1/2}$ = $+0.61$ V. Compared to the oxidation potential of 9-phenylcarbazole at $+0.80$ V, the strong redox wave at the highest potential at $+1.02$ V originates from three carbazolyl groups (E^{CZ}_p). These redox waves were observed reproducibly. In the CV measurements, in a highly polar DMF solution having a wider window to the negative potential, similar redox properties were observed, and the reduction of **1**$^{3-}$ to radical tetraanion (**1**$^{4-}$) can be observed around E^4_p = -2.75 V as an irreversible peak (Fig. S5†). Redox waves corresponding to E^0 to E^4 were also observed in **4** and **5**, and therefore these waves are assignable to the redox processes of the **TOT** skeleton.

According to the molecular orbital (MO) calculations of **1** and **4** (Fig. S6†), the E^1 and E^0 waves correspond to the SOMO and the E^2–E^4 waves correspond to the doubly degenerate LUMOs.[14d] The redox events E^2–E^4 of **1** in DMF are positively shifted by 0.2–0.3 V compared to those of **4** and **5** due to the effective π-extension to the carbazolyl groups (Fig. S5†). The redox potential of E^1 of **1** in CH$_2$Cl$_2$ was slightly higher than that of **5**, and was lower than that of **4** (Fig. S4†). These changes in the redox potentials originating from the substituent effect showed a good agreement with the MO calculation (Table 1 and Fig. S6†). It is known that the electronic effects of the substituent groups are strongly influenced by relative conformation (stereoelectronic chameleon).[24] We also calculated the MO energies of **1** with various dihedral angles between **TOT** and the carbazole moieties (Fig. S7†). The calculation indicates that the increasing dihedral angle causes the weakening of the delocalization of the SOMO and the lowering of the SOMO and LUMO energies. When **TOT** and the carbazolyl groups are co-planar (θ = 0°), the SOMO energy becomes higher, and redox of E^1 of **1** will occur at a lower potential compared to that of **5**. On the other hand, when **TOT** and the carbazolyl groups are vertical to each other (θ = 90°),

the carbazolyl group acts as an electron-withdrawing group, and the redox potential of E^1 of **1** will become higher than that of **4**. The steric repulsion between the hydrogen atoms at the α-positions of **TOT** and 1-positions of the carbazole moieties (H^1 and H^2 in Fig. 3a) causes a twisting between **TOT** and the carbazole moieties. The CV measurements imply that the molecular structure of **1** in the solution state has a twist angle close to that of the optimized structure (θ = 47°).

Absorption spectra

The effects of the introduction of carbazolyl groups into **TOT** neutral radical were further studied by the UV/Vis measurement in CH$_2$Cl$_2$ (Fig. 5). The spectrum of **1** at a shorter wavelength than 700 nm can be explained by the superimposition of the carbazole and **4**. At the longer wavelength region, **1** showed a new strong and broad absorption band with λ_{max} of 1028 nm and ε_{max} of 1.3×10^4 M^{-1} cm^{-1}. In the previous work, we revealed that **TOT** neutral radicals are in an equilibrium between the monomer and π-dimer, and the π-dimer exhibits a low energy absorption band around 800–900 nm due to the strong intermolecular interaction of two SOMOs (indicated by an arrow in Fig. 5).[16] In the temperature dependent measurements from 293–213 K, the intensity of low energy absorption in **1** was almost kept constant at room temperature (Fig. S6†). A similar behavior can be seen in the concentration variable UV/Vis measurement of **1** in CH$_2$Cl$_2$, where the concentration had a negligible effect on the intensity of the low energy absorption band (Fig. S8†). Such a behavior was quite different from those of other **TOT** derivatives, where an increase in temperature and decrease in concentration caused a significant weakening of the band due to the dissociation of the π-dimer (Fig. S9†).[16] These experimental results suggest that the low energy absorption band is caused by the IET from the electron-donating carbazolyl groups to the electron-accepting **TOT** neutral radical.

In order to obtain an insight into the electronic transition, we performed TD-DFT calculations of **1** (Fig. S10†). The calculation reproduced the IET band around 1180 nm originating from the electronic transition from the doubly degenerate
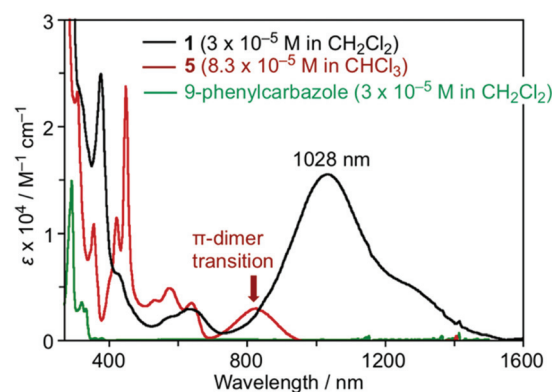
Fig. 5 UV-Vis spectra of **1** (black line), tri-*tert*-butyl **TOT** **5** (brown line), and 9-phenylcarbazole (green line) at room temperature.

3110 | *Org. Chem. Front.*, 2019, **6**, 3107–3115

This journal is © the Partner Organisations 2019

HOMOs to SOMO (Fig. S6†). The HOMO and SOMO coefficients reside on the carbazole and **TOT** parts, respectively. Thus, the calculation also indicates that the low energy absorption band of **1** is an optically induced IET from the carbazolyl group to the **TOT** moiety. The difference between the oxidation potentials of the **TOT** skeleton ($E^1 \sim -0.2$ V) and carbazolyl groups ($E_p^{CZ} = +1.02$ V) in the CV measurements was *ca.* 1.2 V (Fig. 4), corresponding to *ca.* 1000 nm. This value is close to the experimental and calculated IET excitation energy.

A similar absorption band was also observed in the carbazole substituted TTM radicals at around λ_{max} = 600–700 nm with ε_{max} = 2–5 × 10^3 M^{-1} cm^{-1}.[19–21] Since **TOT** possesses a much higher electron-accepting ability than TTM, the transition energy became much smaller. Among the numerous open- and close-shell D–A molecules reported previously, those showing absorption bands at λ_{max} > 1000 nm are rare, and further these bands are weak with $\varepsilon \sim 10^3$ M^{-1} cm^{-1}. In the TTF–TCNQ dyad linked through a σ-bonding linker, a low energy IET band was observed at λ_{max} of 1630 nm with $\varepsilon_{max} \sim 3 × 10^3$ M^{-1} cm^{-1}.[25] The open-shell D–A molecule composed of TTF and 6OPO which has an electron-accepting ability close to that of *p*-chloranil exhibits a very weak IET band at λ_{max} = 1350 nm with $\varepsilon_{max} \sim 6 × 10^2$ M^{-1} cm^{-1}.[10a]

In the low temperature measurements in toluene (3.0 × 10^{-5} M), a weak shoulder band was observed at around 1260 nm, in which the intensity decreased with increasing temperature and almost disappeared at 353 K (Fig. 6). Considering the π-dimerization observed in the temperature dependence of the ESR measurement, this low energy absorption band can be characterized as the intermolecular transition within the π-dimer. Such a behavior is very similar to the π-dimerization of **5**, where the intermolecular transition was observed at λ_{max} = 834 nm.[16] The significant red-shift of **1** in comparison with **5** is caused by the delocalization of the π-electronic system within the molecule. In the solid-state spectrum, the low energy absorption was observed as a single band around 800–1400 nm, where IET and intermolecular transition bands were gathered by broadening (Fig. S11†).
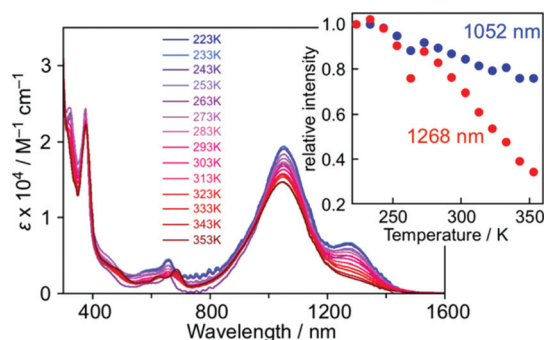
The UV-Vis spectra of **1** were measured in various solvents, where both λ_{max} and intensity of the IET band became lower with increasing the solvent polarity from toluene (1049 nm) to acetonitrile (874 nm) (Fig. 7). The hypsochromic effect of the IET band suggests an increase in the energy gap with the solvent polarity. A similar observation was also found in the PTM radical having a carbazolyl moiety; however, the change in λ_{max} and intensity in carbazole-PTM was remarkably smaller than those of **1**.[26] The difference in the solvent effects between **1** and carbazole-PTM would be the consequence of the stronger electron-accepting ability of the **TOT** moiety compared to that of PTM and/or the extended π-system of **TOT** that enables strong interaction with solvent molecules.

Crystal structure and solid-state properties

A single crystal of **1** was obtained by vapor diffusion using CHCl_3 and EtOH, and the quality of the structural analysis was poor due to the efflorescence of CHCl_3 solvent and disorder of *tert*-butyl groups ($R = 0.15$). The **TOT** skeleton of **1** was nearly planar, and the dihedral angle between the **TOT** and three carbazolyl groups were 42–47° (Fig. 8a). In the crystal packing, **1** formed a π-dimer in a staggered manner with a face-to-face distance of 3.28 Å, similarly to **3** and **4** (stack-A, Fig. 8b).[14d,16] The π-dimers further stacked on the **TOT** and carbazole moieties (stack-B, Fig. 8c, *ca.* 3.2–3.8 Å), forming a one-dimensional chain structure along the *c*-axis (Fig. 8d). Such a stacking pattern is in a sharp contrast with the π-dimer-based columns in the crystal structures of **4** and **5**.[14d,16] This structural feature is probably due to the steric repulsion of the bulky *tert*-butyl groups on the carbazole moiety.

In the temperature dependence of magnetic susceptibility (χ_p, Fig. S12†), almost all spins of **1** were quenched due to the strong antiferromagnetic interaction within the π-dimers shown in the crystal structure (Fig. 8b). The analysis based on the singlet-triplet model[27] resulted in the $2J/k_B$ > −2000 K of antiferromagnetic interaction, which is similar to those in π-dimers of other **TOT** derivatives.[14d] The $2J/k_B$ values of the π-dimer of **1** was also estimated by the DFT method.[28] At the UB3LYP/3-21G level of theory, the calculations showed a $2J/k_B$ value of −2273 K, which is very close to the experimental value. On the other hand, the calculated magnetic interaction

Fig. 6 Temperature-dependent UV-Vis spectra of **1** in toluene (3.0 × 10^{-5} M). The inset shows the plots of the intensities at 1052 nm (blue) and 1268 nm (red), where the values were normalized with those at 223 K.
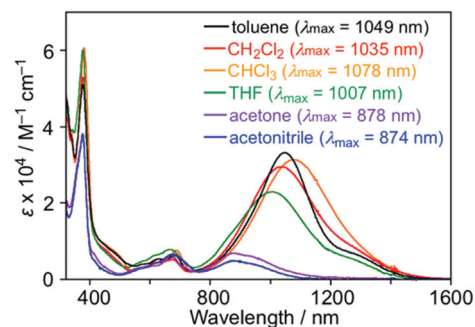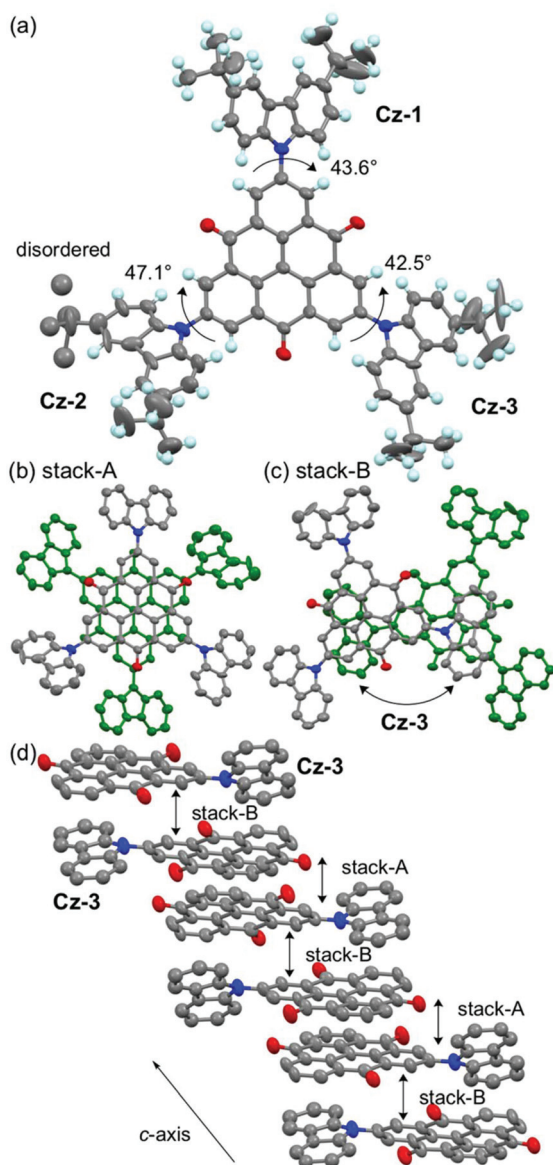

Fig. 7 UV-Vis spectra of **1** in various solvents (∼1.0 × 10^{-5} M) at room temperature. Numerical values in parentheses are λ_{max} of the IET band.

This journal is © the Partner Organisations 2019

Org. Chem. Front., 2019, **6**, 3107–3115 | **3111**

Fig. 8 Crystal structure of **1**. (a) Top view of **1**. Ellipsoids are drawn at the 25% probability level, and labels Cz-A to Cz-C indicate the carbazole moieties. (b, c) Overlap patterns in stacks-A and -B. Hydrogen atoms and *tert*-butyl groups are omitted. (d) 1D π-stacking column along the *c*-axis. Cz-A and -B moieties which do not participate in the π-stacking are omitted.

between the π-dimers was $2J/k_B = -6$ K, much smaller than that within the π-dimer.

Conclusions

In conclusion, we have designed, synthesized and characterized an open-shell D–A molecule, **1**, where three carbazolyl groups were introduced into the **TOT** neutral radical preserving its threefold symmetry. ESR spectroscopy and DFT calculations showed that a large amount of the electronic-spin delocalized over the carbazolyl groups. In the electrochemical measure-

ment, **1** exhibited six-stage redox processes consisting of five steps of **TOT** and one step of the carbazolyl group. Furthermore, **1** exhibited a self-assembling ability to form a π-dimer inherent in **TOT** neutral radicals through strong two-electron-multicentered bonding in both solution and crystalline states. Most importantly, **1** exhibited a strong NIR photo-absorption band both in solution and in the solid state, which was formed by the IET from the carbazolyl groups to the **TOT** neutral radical. The high absorbance of the IET band in the NIR region exceeding 1000 nm is a substantial electronic feature among many D–A molecules.

π-Conjugated molecules showing NIR photoabsorption have been noticed in the research studies not only of organic electronic materials[5,29] but also of biological applications.[30] One of the molecular design strategies for NIR dyes is the extension of the π-conjugated systems as demonstrated in the polymeric fused porphyrin array (3500 nm, dodecamer)[31] and the giant hydrocarbon sheet ($C_{222}H_{42}$, 250–1400 nm).[32] The π-stacking assemblies of open-shell molecules also exhibit NIR absorption bands at 1000–2000 nm as shown in radical-ion salts of TTF and TCNQ[33] and also in **TOT** neutral radicals of our previous studies.[14,15] In both cases, the construction of large π-electronic system through the assembly of many π-units is the key for lowering the absorption energy. The open-shell D–A molecules **1** in the present work realized a strong NIR photoabsorption without extension of the π-electronic system.

Recently, interesting properties and functions of D–A molecules with an open-shell electronic structure have been disclosed. Furthermore, the electronic structures of these systems are sensitive to temperature and solvent, and cause a drastic response on their electronic-spin structures.[10–12] The development of the functionalities of **1** based on the responses to the external stimuli is currently underway. It should also be noted that the one-dimensional π-stacking column of **TOT** neutral radicals exhibits a high electron-transport ability to show a high conductivity in the crystalline state.[15] Our current interest is aimed at the exploration of pressure or NIR photoinduced electrical conductivity as a single component neutral radical crystal or thin film, where IET locally generates $\mathbf{TOT^-}$ species within the one-dimensional column providing a conduction carrier.

Experimental

Materials and methods

The synthesis of compound **2** is described in our previous work.[14c,16] Toluene used for the synthesis and ESR measurement was purified by distillation from CaH_2. R_f values on TLC were acquired on E. Merck precoated (0.25 mm) silica gel 60 F^{254} plates. Melting and decomposition points were measured using hot-stage apparatus with a Yanako MP-J3, and were uncorrected. Melting and/or decomposition were detected by eye observation. Elemental analyses were performed at the Graduate School of Science, Osaka University. [1]H and [13]C

3112 | *Org. Chem. Front.*, 2019, **6**, 3107–3115

This journal is © the Partner Organisations 2019

NMR spectra were obtained on a JEOL ECA-500 with DMSO-d_6 using Me$_4$Si as an internal standard. The infrared spectrum was recorded on a JASCO FT/IR-660 Plus spectrometer using a KBr plate (resolution 4 cm^{-1}).

Synthetic procedures

Synthesis of tetra-*n*-butylammonium 2,6,10-tris[9′-(3′,6′-di-*tert*-butylcarbazolyl)]-4,8-dioxo-4*H*,8*H*-dibenzo[*cd*,*mn*]pyren-12-olate [(*n*-Bu$_4$N$^+$)(1$^-$)]. In a 300 mL Schlenk flask, **2** (700 mg, 1.09 mmol), 3,6-di-*tert*-butylcarbazole (1.22 g, 4.37 mmol), Pd (dba)$_2$ (93.8 mg, 0.16 mmol), tri-*tert*-butylphosphine (36.6 μL, 0.16 mmol), and sodium *tert*-butoxide (471 mg, 4.90 mmol) were placed and dissolved in toluene (70 mL). The resulting mixture was stirred at 100 °C for 47 h, and then cooled down to room temperature. The mixture was diluted with CH$_2$Cl$_2$, and the insoluble material was removed by filtration through the celite column. The filtrate was concentrated under reduced pressure, and then the residue was dissolved in acetone (30 mL). To this mixture was added *n*-Bu$_4$NOH (1 M MeOH solution, 4.0 mL, 4.0 mmol), and the resulting mixture was stirred at 60 °C for 1 h. 2 M HCl aqueous solution was added to the mixture, and the mixture was stirred at 60 °C for 1 h. The resulting precipitate was collected by filtration and washed with water, to give **3** (207 mg, 25%) as a deep purple powder. The product was used in the next reaction without further purification. TLC R_f 0.60 (10 : 1 ethyl acetate/MeOH).

In a 50 mL round-bottomed flask, **3** (80.0 mg, 0.069 mmol) was suspended in acetone (10 mL), and then *n*-Bu$_4$NOH (1 M MeOH solution, 4.0 mL, 4.0 mmol) was added. After stirring at room temperature for 1 h, the mixture was concentrated under reduced pressure. The residue was washed with hot water, and then the resulting precipitate was collected by filtration, to give (*n*-Bu$_4$N$^+$)(**1**$^-$) (94 mg, 97%) as a deep blue powder. M.p. ~280 °C (in air); TLC R_f 0.60 (10 : 1 ethyl acetate/MeOH); ^{1}H NMR (500 MHz, DMSO-d_6, 80 °C) δ 0.94 (m, 12H), 1.28–1.36 (m, 8H), 1.46 (s, 54H), 1.54–1.62 (m, 8H), 3.12–3.18 (m, 8H), 7.50 (s, 12H), 8.32 (s, 6H) 8.90 (s, 6H) ppm; ^{13}C NMR (500 MHz, DMSO-d_6, 80 °C) δ 13.83, 19.76, 23.78, 32.41, 35.05, 58.58, 109.59, 117.07, 123.64, 124.33, 128.84, 130.19, 131.21, 131.65, 139.81, 143.35, 180.31 ppm; IR (KBr) ν 3049, 2961, 2871, 1614, 1548, 1496, 1297 cm^{-1}; UV (CH$_2$Cl$_2$) λ_{max} (ε) 239 (6.0 × 10^4), 291 (4.8 × 10^4), 382 (2.7 × 10^4), 625 (sh, 4.9 × 10^3), 860 (7.2 × 10^3) nm; MALDI-TOFMS (negative-mode) *m/z* 1152.6 ([M − (*n*-Bu)$_4$N]$^-$) (Fig. S13–S15†).

Synthesis of 2,6,10-tris[9′-(3′,6′-di-*tert*-butylcarbazolyl)]-4,8-dioxo-4*H*,8*H*-dibenzo[*cd*,*mn*]pyren-12-olyl [1]. In a 100 mL round-bottomed flask, **3** (76.0 mg, 0.066 mmol) was dissolved in toluene (30 mL). To the solution was added PbO$_2$ (157 mg, 0.66 mmol), and the resulting mixture was stirred at room temperature for 30 min. The reaction mixture was filtered through a celite column. The filtrate was subjected to silica gel column chromatography with toluene as an eluent, to give **1** (71 mg, 94%) as a green powder, which was suitable for the physical property measurements. D.p. >300 °C (in air); TLC R_f 0.70 (10 : 1 hexane/ethyl acetate); IR (KBr) ν 2959, 1639, 1577, 1480, 1372, 1320, 1298 cm^{-1}; UV (CH$_2$Cl$_2$) λ_{max} (ε) 294

(3.7 × 10^4), 376 (2.2 × 10^4), 660 (2.2 × 10^3), 1034 (1.3 × 10^4) nm; UV (KBr) λ_{max} 290, 382, 690, 1064 nm; Anal. Calcd for (C$_{82}$H$_{78}$N$_3$O$_3$)(H$_2$O)$_{0.7}$: C, 85.38; H, 6.82; N, 3.64. Found: C, 84.42; H, 6.96; N, 3.55.

Magnetic measurements

Magnetic resonance measurements were performed on a Bruker ELEXSYS E500 spectrometer for X-band liquid-phase ESR spectra and on Bruker ESR/ENDOR spectrometers ESP 300/350 for ^{1}H-ENDOR, and ^{1}H-TRIPLE spectra equipped with a wide-band 500 W radiofrequency amplifier. The solution of the radical was degassed by the freeze–pump–thaw method before the measurements were recorded. Magnetic susceptibility was measured on a Quantum Design SQUID magnetometer MPMS-XL at 2–300 K. The magnetic responses were corrected with diamagnetic blank data of the sample holder obtained separately. The diamagnetic contribution of the sample itself was estimated from Pascal's constants.

Electrochemical measurements

Electrochemical measurements were made with an ALS Electrochemical Analyzer model 630A. Cyclic voltammograms were recorded with a 3 mm-diameter carbon plate and Pt wire counter electrodes in dry CH$_2$CH$_2$ or DMF containing 0.1 M *n*-Bu$_4$NClO$_4$ as the supporting electrolyte at room temperature. The experiment employed a Ag/AgNO$_3$ reference electrode, and the final results were calibrated with an Fc/Fc$^+$ couple.

UV-Vis absorption spectroscopy

Electronic spectra were measured for KBr pellets or solutions on a Shimadzu UV-vis scanning spectrophotometer UV-3100PC. Temperature-dependent measurements were performed using an Oxford ITC502 temperature controller and an Oxford OptistatDN valuable temperature liquid nitrogen cryostat.

X-ray crystallography

X-ray crystallographic measurements were made on a Rigaku Raxis-Rapid imaging plate with graphite monochromated Cu Kα (λ = 1.54187 Å). The structure was determined by a direct method using SHELXS program,[34] and refinement was performed by a full-matrix least-squares on F^2 using SHELXL-2014.[35] All non-hydrogen atoms were refined anisotropically, and all hydrogen atoms were included but not refined. Empirical absorption correction was applied.

Crystal data for 1. C$_{84}$H$_{80}$Cl$_6$N$_3$O$_3$, M_r = 1392.21, orthorhombic, *Pbcn* (#60), a = 32.108(3) Å, b = 23.7420(7) Å, c = 19.1103(7) Å, V = 14 568(1) Å^3, T = 200 K, Z = 8, d_{calcd} = 1.270 g cm^{-3}, μ = 2.552 mm^{-1}, 2θ_{max} = 136.5°, λ(CuKα) = 1.54187 Å, ω scan mode, 172 468 reflections, of which 13 292 were unique and 3126 were included in the refinement [I > 2.00$\sigma(I)$], data corrected for Lorentzian and polarization effects; an empirical absorption correction resulted in transmission factors ranging from 0.605 to 0.880. The final values R_1 = 0.150, wR_2 = 0.474, GOF = 1.077, maximum positive and negative peaks in ΔF map were ρ_{max} = 0.506 e^{-3} and ρ_{min} = −0.580 e^{-3}. The quality of the

This journal is © the Partner Organisations 2019

Org. Chem. Front., 2019, **6**, 3107–3115 | **3113**

structural analysis was poor due to the efflorescence of the $CHCl_3$ solvent and disorder of *tert*-butyl groups.

Computational details

Density functional theory (DFT) calculations were performed using the Gaussian 03 program package. The calculation of electronic-spin structures of the neutral radicals **1** and **4** was performed at the UB3LYP/6-31G** level of theory with optimization of the geometries. The MO energy levels were calculated at the ROB3LYP/6-31G** level of theory with the geometries obtained from UB3LYP/6-31G**. TD-DFT calculations were performed at the UB3LYP/6-31G** level of theory with the geometries obtained from UB3LYP/6-31G**. In the calculation of intermolecular magnetic interactions within π-stacking structures, the geometries were extracted from the crystal structure, and the UB3LYP/3-21G level of theory was applied.

Conflicts of interest

There are no conflicts of interest to declare.

Acknowledgements

Notes and references

1 (*a*) *Materials for Nonlinear Optics: Chemical Perspectives*, ed. S. R. Marder, J. E. Sohn and G. D. Stucky, ACS Symposium Series 455, American Chemical Society, Washington, DC, 1991; (*b*) R. R. Tykwinski, U. Gubler, R. E. Martin, F. Diederich, C. Bosshard and P. Günter, *J. Phys. Chem. B*, 1998, **102**, 4451.

2 (*a*) D. Gendron and M. Leclerc, *Energy Environ. Sci.*, 2011, **4**, 1225; (*b*) A. Mishra and P. Bäuerle, *Angew. Chem., Int. Ed.*, 2012, **51**, 2020; (*c*) W. Li, K. H. Hendriks, M. M. Wienk and R. A. J. Janssen, *Acc. Chem. Res.*, 2016, **49**, 78; (*d*) K. Nakano and K. Tajima, *Adv. Mater.*, 2017, **29**, 1603269; (*e*) I. Osaka and K. Takimiya, *Adv. Mater.*, 2017, **29**, 1605218.

3 (*a*) H. Fujiwara, Y. Sugishima and K. Tsujimoto, *Tetrahedron Lett.*, 2008, **49**, 7200; (*b*) K. Isoda, T. Yasuda and T. Kato, *Chem. – Asian J.*, 2009, **4**, 1619; (*c*) K. Tsujimoto, R. Ogasawara, Y. Kishi and H. Fujiwara, *New J. Chem.*, 2014, **38**, 406; (*d*) K. Tsujimoto, R. Ogasawara, T. Nakagawa and H. Fujiwara, *Eur. J. Inorg. Chem.*, 2014, 3960; (*e*) Y. Beldjoudi, M. A. Nascimento, Y. J. Cho, H. Yu, H. Aziz, D. Tonouchi, K. Eguchi, M. M. Matsushita, K. Awaga, I. Osorio-Roman, C. P. Constantinides and J. M. Rawson, *J. Am. Chem. Soc.*, 2018, **140**, 6260.

4 (*a*) H. Chiba, J. Nishida and Y. Yamashita, *Chem. Lett.*, 2012, **41**, 482; (*b*) J. Fan, J. D. Yuen, M. Wang, J. Seifter, J.-H. Seo, A. R. Mohebbi, D. Zakhidov, A. Heeger and F. Wudl, *Adv. Mater.*, 2012, **24**, 2186; (*c*) J. D. Yuen and F. Wudl, *Energy Environ. Sci.*, 2013, **6**, 392.

5 (*a*) J. Fabian, H. Nakazumi and M. Matsuoka, *Chem. Rev.*, 1992, **92**, 1197; (*b*) G. Qian and Z. Y. Wang, *Chem. – Asian J.*, 2010, **5**, 1006; (*c*) Z. Y. Wang, *Near-infrared organic materials and emerging applications*, CRC Press, Boca Raton, FL, 2013.

6 (*a*) M. Tian, S. Tatsuura, M. Furuki, Y. Sato, I. Iwasa and L. S. Pu, *J. Am. Chem. Soc.*, 2003, **125**, 348; (*b*) G. Qian, B. Dai, M. Luo, D. Yu, J. Zhan, Z. Zhang, D. Ma and Z. Y. Wang, *Chem. Mater.*, 2008, **20**, 6208; (*c*) M. Luo, H. Shadnia, G. Qian, X. Du, D. Yu, D. Ma, J. S. Wright and Z. Y. Wang, *Chem. – Eur. J.*, 2009, **15**, 8902; (*d*) G. Qian and Z. Y. Wang, *Can. J. Chem.*, 2010, **88**, 192.

7 Several π-conjugated polymers of D–A molecules showing NIR absorption bands have been reported: (*a*) Y. Wang and T. Michinobu, *J. Mater. Chem. C*, 2016, **4**, 6200; (*b*) T. T. Steckler, P. Henriksson, S. Mollinger, A. Lundin, A. Salleo and M. R. Andersson, *J. Am. Chem. Soc.*, 2014, **136**, 1190.

8 (*a*) M. Souto, H. Cui, M. Peña-Álvarez, V. G. Baonza, H. O. Jeschke, M. Tomic, R. Valentí, D. Blasi, I. Ratera, C. Rovira and J. Veciana, *J. Am. Chem. Soc.*, 2016, **138**, 11517; (*b*) M. Souto, C. Rovira, I. Ratera and J. Veciana, *CrystEngComm*, 2017, **19**, 197; (*c*) M. Souto, M. C. Gullo, H. Cui, N. Casati, F. Montisci, H. O. Jeschke, R. Valentí, I. Ratera, C. Rovira and J. Veciana, *Chem. – Eur. J.*, 2018, **24**, 5500.

9 H. Komatsu, M. M. Matsushita, S. Yamamura, Y. Sugawara, K. Suzuki and T. Sugawara, *J. Am. Chem. Soc.*, 2010, **132**, 4528.

10 (*a*) S. Nishida, Y. Morita, K. Fukui, K. Sato, D. Shiomi, T. Takui and K. Nakasuji, *Angew. Chem., Int. Ed.*, 2005, **44**, 7277; (*b*) S. Nishida, K. Fukui and Y. Morita, *Chem. – Asian J.*, 2014, **9**, 500.

11 (*a*) J. Guasch, L. Grisanti, V. Lloveras, J. Vidal-Gancedo, M. Souto, D. C. Morales, M. Vilaseca, C. Sissa, A. Painelli, I. Ratera, C. Rovira and J. Veciana, *Angew. Chem., Int. Ed.*, 2012, **51**, 11024; (*b*) J. Guasch, L. Grisanti, M. Souto, V. Lloveras, J. Vidal-Gancedo, I. Ratera, A. Painelli, C. Rovira and J. Veciana, *J. Am. Chem. Soc.*, 2013, **135**, 6958.

12 (*a*) I. Ratera, D. Ruiz-Molina, F. Renz, J. Ensling, K. Wurst, C. Rovira, P. Gütlich and J. Veciana, *J. Am. Chem. Soc.*,

3114 | *Org. Chem. Front.*, 2019, **6**, 3107–3115

This journal is © the Partner Organisations 2019

2003, **125**, 1462; (*b*) J. Guasch, L. Grisanti, S. Jung, D. Morales, G. D'Avino, M. Souto, X. Fontrodona, A. Painelli, F. Renz, I. Ratera and J. Veciana, *Chem. Mater.*, 2013, **25**, 808.

13 X. Wu, J. O. Kim, S. Medina, F. J. Ramírez, P. M. Burrezo, S. Wu, Z. L. Lim, C. Lambert, J. Casado, D. Kim and J. Wu, *Chem. – Eur. J.*, 2017, **23**, 7698.

14 (*a*) Y. Morita, S. Suzuki, K. Sato and T. Takui, *Nat. Chem.*, 2011, **3**, 197; (*b*) Y. Morita, S. Nishida, T. Murata, M. Moriguchi, A. Ueda, M. Satoh, K. Arifuku, K. Sato and T. Takui, *Nat. Mater.*, 2011, **10**, 947; (*c*) T. Takui, K. Sato and Y. Morita, *WO. Pat*, WO2013042706A1, 2013; (*d*) Y. Morita, T. Murata, A. Ueda, C. Yamada, Y. Kanzaki, D. Shiomi, K. Sato and T. Takui, *Bull. Chem. Soc. Jpn.*, 2018, **91**, 922; (*e*) T. Murata, N. Asakura, S. Ukai, A. Ueda, Y. Kanzaki, K. Sato, T. Takui and Y. Morita, *ChemPlusChem*, 2019, **84**, 680; (*f*) H. Enozawa, S. Ukai, H. Ito, T. Murata and Y. Morita, *Org. Lett.*, 2019, **21**, 2161; (*g*) T. Murata, K. Kotsuki, H. Murayama, R. Tsuji and Y. Morita, *Commun. Chem.*, 2019, **2**, 46.

15 T. Murata, C. Yamada, K. Furukawa and Y. Morita, *Commun. Chem.*, 2018, **1**, 47.

16 Y. Ikabata, Q. Wang, T. Yoshikawa, A. Ueda, T. Murata, K. Kariyazono, M. Moriguchi, H. Okamoto, Y. Morita and H. Nakai, *npj Quantum Mater.*, 2017, **2**, 27.

17 (*a*) J. F. Ambrose and R. F. Nelson, *J. Electrochem. Soc.*, 1968, **115**, 1159; (*b*) D. R. Prudhomme, Z. Wang and C. J. Rizzo, *J. Org. Chem.*, 1997, **62**, 8257; (*c*) Z. Gomurashvili, Y. Hua and J. V. Crivello, *Macromol. Chem. Phys.*, 2001, **202**, 2133; (*d*) M. Sangermano, G. Malucelli, A. Priola, S. Lengvinaite, J. Simokaitiene and J. V. Grazulevicius, *Eur. Polym. J.*, 2005, **41**, 475; (*e*) S.-K. Chiu, Y.-C. Chung, G.-S. Liou and Y. O. Su, *J. Chin. Chem. Soc.*, 2012, **59**, 1.

18 (*a*) V. I. Adamovich, S. R. Cordero, P. I. Djurovich, A. Tamayo, M. E. Thompson, B. W. D'Andrade and S. R. Forrest, *Org. Electron.*, 2003, **4**, 77; (*b*) A. van Dijken, J. J. A. M. Bastiaansen, N. M. M. Kiggen, B. M. W. Langeveld, C. Rothe, A. Monkman, I. Bach, P. Stössel and K. Brunner, *J. Am. Chem. Soc.*, 2004, **126**, 7718; (*c*) J. F. Morin, N. Drolet, Y. Tao and M. Leclerc, *Chem. Mater.*, 2004, **16**, 4619; (*d*) K. R. Justin Thomas, M. Velusamy, J. T. Lin, Y. T. Tao and C. H. Chuen, *Adv. Funct. Mater.*, 2004, **14**, 387; (*e*) K. Brunner, A. V. van Dijken, H. Borner, J. J. A. M. Bastiaansen, N. M. M. Kiggen and B. M. W. Langeveld, *J. Am. Chem. Soc.*, 2004, **126**, 6035.

19 (*a*) V. Gamero, D. Velasco, S. Latorre, F. López-Calahorra, E. Brillas and L. Juliá, *Tetrahedron Lett.*, 2006, **47**, 2305;

(*b*) J. V. Grazulevicius, P. Strohriegl, J. Pielichowski and K. Pielichowski, *Prog. Polym. Sci.*, 2003, **28**, 1297; (*c*) K. Parimal, K. R. Justin Thomas, T. L. Jiann, Y. T. Tao and C. H. Chien, *Adv. Funct. Mater.*, 2003, **13**, 445; (*d*) B. Akira, O. Ken, K. Wolfgang and C. A. J. Rigoberto, *Phys. Chem. B*, 2004, **108**, 18949.

20 (*a*) S. Castellanos, D. Velasco, F. López-Calahorra, E. Brillas and L. Julia, *J. Org. Chem.*, 2008, **73**, 3759; (*b*) S. Castellanos, L. López-Calahorra, E. Brillas, L. Julia and D. Velasco, *Angew. Chem., Int. Ed.*, 2009, **48**, 6516.

21 (*a*) S. Castellanos, V. Gaidelis, V. Jankauskas, J. V. Grazulevicius, E. Brillas, F. López-Calahorra, L. Juliá and D. Velasco, *Chem. Commun.*, 2010, **46**, 5130; (*b*) M. Reig, C. Gozalvez, V. Jankauskas, V. Gaidelis, J. V. Grazulevicius, L. Fajarí, L. Juliá and D. Velasco, *Chem. – Eur. J.*, 2016, **22**, 18551.

22 J. F. Hartwig, M. Kawatsura, S. I. Hauck, K. H. Shaughnessy and L. M. Alcazar-Roman, *J. Org. Chem.*, 1999, **64**, 5575.

23 D. Small, V. Zaitsev, Y. Jung, S. V. Rosokha, M. Head-Gordon and J. K. Kochi, *J. Am. Chem. Soc.*, 2004, **126**, 13850.

24 S. Z. Vatsadze, Y. D. Loginova, G. dos Passos Gomes and I. V. Alabugin, *Chem. – Eur. J.*, 2017, **23**, 3225.

25 D. F. Perepichka, M. R. Bryce, C. Pearson, M. C. Petty, E. J. L. McInnes and J. P. Zhao, *Angew. Chem., Int. Ed.*, 2003, **42**, 4636.

26 A. Gilabert, L. Fajarí, I. Sirés, M. Reig, E. Brillas, D. Velasco, J. M. Anglada and L. Juliá, *New J. Chem.*, 2017, **41**, 8422.

27 B. Bleaney and K. D. Bowers, *Proc. R. Soc. London, Ser. A*, 1952, **214**, 451.

28 Y. Takano, T. Taniguchi, H. Isobe, T. Kubo, Y. Morita, K. Yamamoto, K. Nakasuji, T. Takui and K. Yamaguchi, *J. Am. Chem. Soc.*, 2002, **124**, 11122.

29 Z. Sun, Q. Ye, C. Chi and J. Wu, *Chem. Soc. Rev.*, 2012, **41**, 7857.

30 A. Alabugin, *Photochem. Photobiol.*, 2019, **95**, 722.

31 (*a*) A. Tsuda and A. Osuka, *Science*, 2001, **293**, 79; (*b*) H. Mori, T. Tanaka and A. Osuka, *J. Mater. Chem. C*, 2013, **1**, 2500.

32 C. D. Simpson, J. D. Brand, A. J. Berresheim, L. Przybilla, H. J. Räder and K. Müllen, *Chem. – Eur. J.*, 2002, **8**, 1424.

33 (*a*) J. B. Torrance, B. A. Scott, B. Welber, F. B. Kaufman and P. E. Seiden, *Phys. Rev. B*, 1979, **19**, 730; (*b*) J. B. Torrance, *Acc. Chem. Res.*, 1979, **12**, 79; (*c*) S. Yamaguchi, Y. Moritomo and Y. Tokura, *Phys. Rev. B*, 1993, **48**, 6654; (*d*) M. Meneghetti, *Phys. Rev. B*, 1994, **50**, 16899.

34 G. M. Sheldrick, *Acta Crystallogr., Sect. A*, 2008, **64**, 112.

35 G. M. Sheldrick, *Acta Crystallogr., Sect. C*, 2015, **71**, 3.

This journal is © the Partner Organisations 2019

Org. Chem. Front., 2019, **6**, 3107–3115 | **3115**